

Protein profile of *Beta vulgaris* leaf apoplastic fluid and changes induced by Fe deficiency and Fe resupply

Laura Ceballos-Laita¹, Elain Gutierrez-Carbonell¹, Giuseppe Lattanzio¹, Saul Vázquez¹, Bruno Contreras-Moreira^{2,3}, Anunciación Abadía¹, Javier Abadía¹ and Ana-Flor López-Millán^{1*}

¹ Plant Stress Physiology Group, Department of Plant Nutrition, Aula Dei Experimental Station, Consejo Superior de Investigaciones Científicas, Zaragoza, Spain, ² Laboratory of Computational and Structural Biology, Aula Dei Experimental Station, Consejo Superior de Investigaciones Científicas, Zaragoza, Spain, ³ Fundación ARAID, Zaragoza, Spain

OPEN ACCESS

Edited by:

Jesus V. Jorrin Novo,
University of Cordoba, Spain

Reviewed by:

Natalia V. Bykova,
Agriculture and Agri-Food Canada,
Canada
Jesus V. Jorrin Novo,
University of Cordoba, Spain
Arkadiusz Kosmala,
Institute of Plant Genetics of the Polish
Academy of Sciences, Poland

*Correspondence:

Ana-Flor López-Millán,
Aula Dei Experimental Station,
Consejo Superior de Investigaciones
Científicas, Department of Plant
Nutrition, Avenida Montañana 1005,
50059 Zaragoza, Spain
anaflor@eead.csic.es

Specialty section:

This article was submitted to Plant
Proteomics, a section of the journal
Frontiers in Plant Science

Received: 30 December 2014

Accepted: 23 February 2015

Published: 18 March 2015

Citation:

Ceballos-Laita L, Gutierrez-Carbonell
E, Lattanzio G, Vázquez S,
Contreras-Moreira B, Abadía A,
Abadía J and López-Millán A-F (2015)
Protein profile of *Beta vulgaris* leaf
apoplastic fluid and changes induced
by Fe deficiency and Fe resupply.
Front. Plant Sci. 6:145.
doi: 10.3389/fpls.2015.00145

The fluid collected by direct leaf centrifugation has been used to study the proteome of the sugar beet apoplastic fluid as well as the changes induced by Fe deficiency and Fe resupply to Fe-deficient plants in the protein profile. Plants were grown in Fe-sufficient and Fe-deficient conditions, and Fe resupply was carried out with 45 μ M Fe(III)-EDTA for 24 h. Protein extracts of leaf apoplastic fluid were analyzed by two-dimensional isoelectric focusing-SDS-PAGE electrophoresis. Gel image analysis revealed 203 consistent spots, and proteins in 81% of them (164) were identified by nLC-MS/MS using a custom made reference repository of beet protein sequences. When redundant UniProt entries were deleted, a non-redundant leaf apoplastic proteome consisting of 109 proteins was obtained. TargetP and SecretomeP algorithms predicted that 63% of them were secretory proteins. Functional classification of the non-redundant proteins indicated that stress and defense, protein metabolism, cell wall and C metabolism accounted for approximately 75% of the identified proteome. The effects of Fe-deficiency on the leaf apoplast proteome were limited, with only five spots (2.5%) changing in relative abundance, thus suggesting that protein homeostasis in the leaf apoplast fluid is well-maintained upon Fe shortage. The identification of three chitinase isoforms among proteins increasing in relative abundance with Fe-deficiency suggests that one of the few effects of Fe deficiency in the leaf apoplast proteome includes cell wall modifications. Iron resupply to Fe deficient plants changed the relative abundance of 16 spots when compared to either Fe-sufficient or Fe-deficient samples. Proteins identified in these spots can be broadly classified as those responding to Fe-resupply, which included defense and cell wall related proteins, and non-responsive, which are mainly protein metabolism related proteins and whose changes in relative abundance followed the same trend as with Fe-deficiency.

Keywords: leaf apoplast, iron deficiency, proteome, sugar beet, two-dimensional electrophoresis

Introduction

Iron is the fourth most abundant element in the earth's crust and it is an essential micronutrient for all living organisms including plants. However, its low availability in neutral or alkaline soils, which

account for approximately 30% of the world's arable soils, causes Fe deficiency (Abadía et al., 2004). Iron deficiency is the most common nutritional disorder in many plants and typical symptoms include chlorosis of young leaves (leaf yellowing) and reduced crop yield and quality, which result in increased orchard management costs (Álvarez-Fernández et al., 2006; Rombolà and Tagliavini, 2006; Abadía et al., 2011).

Plants have developed two main mechanisms to allow Fe uptake from the soil: a strategy based on Fe (III) chelation (Strategy II) used by graminaceous plants, and a strategy used by non-graminaceous plants based on Fe(III) reduction (Strategy I) (Römheld and Marschner, 1986; Curie and Briat, 2003; Abadía et al., 2011). When challenged with Fe shortage, Strategy I plants such as *Beta vulgaris* increase the activity of several enzymes at the root plasma membrane level. These changes are aimed at increasing Fe uptake and include increases in a Fe(III) reductase (FRO, Ferric Reductase Oxidase; Robinson et al., 1999), an Fe transporter (IRT1, Iron Regulated Transporter) which introduces Fe(II) into the root cell (Eide et al., 1996; Fox and Guerinot, 1998) and an H⁺-ATPase that lowers the pH of the rhizosphere increasing soil Fe solubility (Santi et al., 2005; Santi and Schmidt, 2008, 2009). Also, several changes occur at the metabolic level in order to support the increased demand of energy and reducing power of Fe-deficient Strategy I roots (Zocchi, 2006). These changes include increased activity of the glycolytic pathway and TCA cycle, shifts in the redox state of the cytoplasm and in the mitochondrial electron transport chain (Schmidt, 1999; López-Millán et al., 2000b; Zocchi, 2006; Vigani, 2012).

While it is well-known that Fe is transported to the shoot *via* xylem, complexed by citrate (López-Millán et al., 2000a; Rellán-Álvarez et al., 2010), the mechanisms for Fe loading and unloading from the vasculature system are not yet fully understood. These processes could take place *via* parenchyma cells or by passive diffusion to the apoplastic space driven by transpiration (Abadía et al., 2011). Also, Fe uptake by mesophyll cells is not as well-studied as in roots. An Fe-reductase activity has been detected in leaf cells and protoplasts (Nikolic and Römheld, 1999; González-Vallejo et al., 2000; Jeong and Connolly, 2009) and AtFRO6 has been located in leaf PM-membranes (Mukherjee et al., 2006; Jeong et al., 2008). However, *fro6* mutant plants do not display any Fe-deficiency symptoms (Jeong and Connolly, 2009) therefore suggesting the existence of other reducing mechanisms. Factors such as differences in apoplastic pH and carboxylate concentrations as a result of Fe deficiency may also regulate leaf Fe reductase activity. On the other hand, light has also been proposed to directly photoreduce Fe (III)-citrate complexes in the leaf apoplast (Nikolic and Römheld, 2007).

The apoplast is a free diffusional space outside the plasma membrane that occupies less of 5% of the plant tissue volume in aerial organs (Steudle et al., 1980; Parkhurst, 1982) and the root cortex (Vakhmistrov, 1967). Among other important functions, such as transport and storage of minerals (Starrach and Mayer, 1989; Wolf et al., 1990; Zhang et al., 1991) or signal transmission (Hartung et al., 1992), the apoplast plays a major role in plant defense (Pechanova et al., 2010). Given that the composition of the apoplastic fluid results from the balance between xylem

and phloem transport and mesophyll cell uptake processes, small changes in these fluxes could produce large changes in the solute concentrations in the apoplast. Changes in the apoplastic composition have been described in biotic and abiotic stresses such as Fe deficiency, air pollutants, heavy metal toxicity, drought, salinity, and extreme temperature (Griffith et al., 1992; Brune et al., 1994; Covarrubias et al., 1995; Dietz, 1997; López-Millán et al., 2000a; Fecht-Christoffers et al., 2003). For instance, Fe deficiency causes a slight decrease in the pH of the apoplast and has a strong impact on the carboxylate composition, with major increases in the concentrations of citrate and malate (López-Millán et al., 2000a). These Fe-deficiency induced changes in the leaf apoplast chemical environment have been suggested to play a role in Fe homeostasis (López-Millán et al., 2000a).

Apoplastic fluid isolation is always carried out using some degree of force (e.g., vacuum perfusion, leaf centrifugation, or pressure using a Schölander bomb), therefore leading to the presence of some cytosolic components in the samples (Lohaus et al., 2001). This contamination may be originated by the rupture of a certain fraction of the leaf mesophyll cells, or, alternatively, by the rupture of the plasmodesmata that communicate neighboring cells. The degree of contamination is usually assessed using cellular marker enzymes such as cytosolic malate dehydrogenase (c-mdh) or other cytoplasmic or internal organelle components, with values ≤3% considered acceptable (Dannel et al., 1995; Lohaus et al., 2001).

Proteomic approaches are useful to understand the general effect that a given stress exerts on metabolic processes (Jorrín-Novo et al., 2009). These approaches have been previously used to study the effects of Fe deficiency in several plant tissues, including thylakoids and roots (López-Millán et al., 2013). Most of the leaf apoplastic proteomic studies so far have been devoted to the study of the protein profile or the effect of biotic stresses. However, knowledge about the effects of nutritional stresses such as Fe deficiency in the apoplastic fluid protein profile is still very limited. Therefore, the aim of this study was first to obtain an overview of the leaf apoplast proteome in sugar beet plants and second to characterize the changes induced by Fe deficiency and resupply in the protein profile of this compartment, with the final goal of shedding light into the major processes taking place in the apoplast and the effect of Fe deficiency on them.

Material and Methods

Plant Material and Growth Conditions

Sugar beet (*Beta vulgaris* L. cv. Orbis) was grown in a growth chamber with a photosynthetic photon flux density (PPFD) of 350 μmol m⁻² s⁻¹ PAR, 80% relative humidity and a photoperiod of 16 h, 23°C/8 h, 18°C day/night regime. Seeds were germinated and grown in vermiculite for 2 weeks. Seedlings were grown for an additional 2 weeks period in half-strength Hoagland nutrient solution with 45 μM Fe(III)-EDTA, and then transplanted to 20 L plastic buckets (four plants per bucket) containing half-strength Hoagland nutrient solution with either 0 or 45 μM Fe(III)-EDTA. Iron-free nutrient solutions were buffered at pH 7.7 with 1 mM NaOH and 1 g L⁻¹ of CaCO₃. Young leaves from

plants grown for 10 d in the presence and absence of Fe were used to collect the apoplastic fluid in all experiments. In the Fe-resupply experiment, 45 μM Fe (III)-EDTA was added to the nutrient solution of plants grown for 10 d in the absence of Fe. The apoplastic fluid of these plants was collected 24 h after Fe addition.

Experimental Design

The experiment was repeated four times with independent sets of plants. Each batch of plants consisted of four buckets per treatment with four plants per bucket. Apoplastic fluid was isolated from the four to five youngest leaves of each plant. Cytosolic contamination was assayed in each sample as described below. Samples with less than 3% of cytosolic contamination from a given treatment per batch were pooled together and considered as a biological replicate ($n = 4$).

Collection of Leaf Apoplastic Fluid

Leaf apoplastic fluid was obtained from whole sugar beet leaves by direct centrifugation (López-Millán et al., 2000a). Briefly, leaves were excised at the base of the petiole and each leaf was rolled and placed into a plastic syringe barrel. Leaf-filled syringes were first centrifuged at low speed (2500 g, 4°C, 15 min) to remove the xylem sap from the main vein and the fluid collected was discarded. A second centrifugation was then carried out at 4°C, 4000 g for 15 min and the fluid collected was considered as soluble apoplastic fluid. The activity of cytosolic malate dehydrogenase (c-mdh; EC 1.1.1.37) in the collected fluid was measured immediately and used as a cytosolic contamination marker. The activity of c-mdh was measured spectrophotometrically at 340 nm in a final reaction mixture containing 46.5 mM Tris (pH 9.5), 0.1 mM NADH, 0.4 mM oxaloacetate and 5 μL of apoplastic fluid and referred to activity measured in a whole leaf extract (López-Millán et al., 2000a). For the activity in whole leaf extracts, approximately 0.1 g of leaf tissue was homogenized with 2 mL of a buffer (pH 8.0) containing 100 mM HEPES, 30 mM sorbitol, 2 mM DTT, 1 mM CaCl_2 , 1% (w/v) bovine serum albumin and 1% (w/v) polyvinylpyrrolidone. The supernatant was collected and analyzed immediately after a 10 min centrifugation at 10,000 g.

Protein Extraction

Proteins in approximately 1 mL of apoplastic fluid were precipitated by adding five volumes of cold 10% TCA. Samples were incubated for at least 14 h at 4°C and then centrifuged at 10,000 g for 15 min. The pellet was washed twice with cold methanol, dried with N_2 gas and solubilized in a sample rehydration buffer containing 8 M urea, 2% (w/v) CHAPS, 50 mM DTT, 2 mM PMSF and 0.2% (v/v) IPG buffer pH 3–10 (GE Healthcare, Uppsala, Sweden). After rehydration, samples were incubated in a Thermomixer Confort device (Eppendorf AG, Hamburg, Germany) at 29°C and 1000 rpm during 3 h, then centrifuged at 10,000 \times g for 10 min at RT and filtered (0.45 μm ultrafree-MC filters, Millipore, Bedford, USA). Protein concentration in the samples was quantified immediately with the Bradford method in microtiter plates using an Asys UVM 340 spectrophotometer (Biochrom Ltd., Cambridge, UK) and BSA as standard.

2-DE

A first dimension IEF separation was carried out on 7 cm ReadyStrip IPG Strips (BioRad, Hercules, CA, USA) with a linear pH gradient 3–10 in a Protean IEF Cell (BioRad). Strips were passively rehydrated for 16 h at 20°C in 125 μL of rehydration buffer containing 80 μg of apoplast proteins and a trace of bromophenol blue and then strips were transferred onto a strip electrophoresis tray. IEF was run at 20°C, for a total of 14,000 V h (20 min with 0–250 V linear gradient; 2 h with 250–4000 V linear gradient and 4000 V until 10,000 V h). After IEF, strips were equilibrated for 10 min in equilibration solution I [6 M urea, 0.375 M Tris-HCl, pH 8.8, 2% (w/v) SDS, 20% (v/v) glycerol, 2% (w/v) DTT] and for another 10 min in equilibration solution II [6 M urea, 0.375 M Tris-HCl pH 8.8, 2% (w/v) SDS, 20% (v/v) glycerol, 2.5% (w/v) iodoacetamide]. For the second dimension, polyacrylamide gel electrophoresis (SDS-PAGE) and equilibrated IPG strips were placed on top of vertical 12% SDS-polyacrylamide gels (8 \times 10 \times 0.1 cm) and sealed with melted 0.5% agarose in 50 mM Tris-HCl (pH 6.8) containing 0.1% SDS. SDS-PAGE was carried out at 20 mA per gel for approximately 1.5 h at 4°C, until the bromophenol blue reached the plate bottom, in a buffer containing 25 mM Tris Base, 192 mM glycine, and 0.1% SDS. Gels were subsequently stained with Coomassie blue G-250 (Serva, Barcelona, Spain). For each treatment, gels were made from four independent apoplast protein extracts ($n = 4$), each of them obtained by pooling the apoplastic fluid collected from 5 to 6 leaves in a given batch.

Gel Image and Statistical Analysis

Stained gels were scanned with an Epson Perfection 4990 Photo Scanner (Epson Ibérica, Barcelona, Spain), previously calibrated using the SilverFast 6 software (LaserSoft Imaging AG, Kiel, Germany) using an IT8 reference card. Experimental MR values were calculated by mobility comparisons with Precision Plus protein standard markers (BioRad) run in a separate lane on the SDS-gel, and pI was determined by using a 3–10 linear scale over the total dimension of the IPG strips. Spot detection, gel matching and interclass analysis were performed with PDQuest 8.0 software (BioRad). Normalized spot volumes based on total intensity of valid spots were calculated for each 2-DE gel and used for statistical calculations of protein abundance; for all spots present in the gels, pI, Mr, and normalized volumes (mean values and SD) were determined. Only spots present in all four replicates from at least one treatment were considered as consistent and used in further analysis. The spots were also manually checked, and a high level of reproducibility between normalized spot volumes was found in all four different replicates.

Univariate and multivariate statistical analyses were carried out. Protein response ratios were defined as the relative abundance in a given treatment divided by the relative abundance in the control; when ratios were lower than one the inverse was taken and the sign changed. Spots changing in relative abundance were defined using a Student *t*-test and a significance level of $p < 0.05$. Among these, only protein species with mean response ratios above 2.0 or below -2.0 were considered relevant and are discussed in this study. Principal component analysis (PCA) analysis was also carried out, using Statistical software (v. 10.0)

and including only those spots showing differential accumulation as a result of the Fe-deficiency and Fe-resupply treatments.

Protein in Gel Digestion

Consistent spots were excised automatically using a spot cutter EXQuest (BioRad), transferred to 500 μL Protein LoBind Eppendorf tubes, destained in 400 μL of 40% [v/v] acetonitrile (ACN) and 60% [v/v] 200 mM NH_4HCO_3 for 30 min and dehydrated in 100% ACN for 10 min. Gel pieces were dried at RT and then *in gel* digested with 15 μL Trypsin solution (Sequencing Grade Modified Trypsin V511, Promega, Madison, WI, US; 0.1 $\mu\text{g } \mu\text{L}^{-1}$ in 40 mM NH_4HCO_3 /9% ACN). After incubation for 5 h at 37°C, the reaction was stopped by adding 1 μL of 1% TFA. The peptide solution was finally analyzed using mass spectrometry (MS).

Reference Repository of Beet Protein Sequences

Proteomes of five sequenced beet accessions (RefBeet, KDHBv, YMoBv, UMSBv and YTiBv) were downloaded from <http://bvseq.molgen.mpg.de/Genome/Download>, corresponding to gene models annotated as of February 2013. In addition, all *B. vulgaris* protein sequences annotated in Uniprot (www.uniprot.org) were retrieved, and added to the set, which was subsequently filtered to remove redundant sequences with software CD-HIT (<http://www.ncbi.nlm.nih.gov/pubmed/23060610>) with cutoff -c 1.0 and otherwise default parameters. The final non-redundant set contained 82,368 protein sequences.

Protein Identification by Nano-Liquid Chromatography-Tandem Mass Spectrometry (nLC-ESI-MS/MS)

Peptides present in 6 μL of sample were pre-concentrated on line onto a 300 μm i.d. \times 5 mm, 5 μm particle size ZORBAX 300SB-C18 trap column (Agilent Technologies, Waldbronn, Germany), using a 100 $\mu\text{L min}^{-1}$ flow rate of 3% ACN, 0.1% formic acid, in a nano-HPLC system 1200 series (Agilent Technologies). Backflow elution of peptides from the trap column was carried out, and separation was done with a 75 μm i.d. \times 150 mm, 3.5 μm particle size ZORBAX 300SB-C18 column (Agilent Technologies), using a 300 nL min^{-1} nano-flow rate and a 55 min linear gradient from solution 97% A (0.1% formic acid) to 90% of solution B (90% ACN, 0.1% formic acid). The nano-HPLC was connected to a HCT Ultra high-capacity ion trap (Bruker Daltonik, Bremen, Germany) using a PicoTip emitter (50 μm i.d., 8 μm tip i.d., New Objective, Woburn, MA, USA) and an on line nano-electrospray source. Capillary voltage was \times 1.8 kV in positive mode and a dry gas flow rate of 10 L min^{-1} was used with a temperature of 180°C. The scan range used was from 300 to 1500 m/z. The mass window for precursor ion selection was \pm 0.2 Da and the rest of parameters were those recommended by the manufacturer for MS/MS proteomics work. Peak detection, deconvolution and processing were performed with Data Analysis 3.4 software (Bruker Daltonik).

Protein identification was carried out using the Mascot search engine v. 2.5.0 (Matrix Science; London, UK) and the non-redundant *B. vulgaris* 20140811 (82,368 sequences; 28,127,547 residues), NCBI 20130310 (23,641,837 sequences; 8,123,359,852 residues), and Plants_EST EST_114 20140804

(158,278,518 sequences; 27,948,288,346 residues). Search parameters were: monoisotopic mass accuracy, peptide mass tolerance \pm 0.2 Da, fragment mass tolerance \pm 0.6 Da, one allowed missed cleavage, fixed modification carbamidomethylation (Cys), and variable modification oxidation (Met). Positive identification was assigned with Mascot *P*-values below the threshold ($p < 0.05$), at least two identified peptides with a score above homology, 10% sequence coverage and similar experimental and theoretical MW and pI values. We used the GO biological process annotation (<http://www.geneontology.org>) for classification of each individual protein identified. The secretion of apoplastic proteins was predicted using TargetP (www.cbs.dtu.dk/services/TargetP) (Emanuelsson et al., 2007), and SecretomeP (www.cbs.dtu.dk/services/SecretomeP) analysis to predict classical and non-classical secreted proteins, respectively (Bendtsen et al., 2004, 2005).

Quantitative RT-PCR

Expression of chitinase and thaumatin genes was analyzed by qRT-PCR in two batches of plants. Total RNA from *B. vulgaris* leaves was isolated using the RNeasy Plant mini kit from QIAGEN (QIAGEN Inc., Valencia, CA, USA) according to the manufacturer's instructions. Samples were treated with DNase (recombinant DNase from Macherey-Nagel, Düren, Germany) to remove contaminating genomic DNA. The concentration of RNA and cDNA was determined with a Nanodrop system (Thermo Fisher Scientific, Waltham, MA, USA) and the structural integrity the RNA was checked using non-denaturing agarose gel stained with SybrSafe (Invitrogen, Carlsbad, CA, USA). One μg of total RNA was reverse transcribed to cDNA by using the SuperScript III reverse transcriptase and 2.5 μM poly(dT)₂₀ primer in a final volume of 20 μl according to the manufacturer's instructions (Invitrogen, Carlsbad, CA, USA). Quantitative real time polymerase chain reactions were performed in a AB7500 Fast Real-Time PCR system (Applied Biosystems by Life Technologies, Grand Island, New York) with equal amount of cDNA for all samples and 10 μl SYBR green master mix (Applied Biosystems, Warrington, UK) using gene specific primers and two different housekeeping genes (actin and tubulin) in a final volume of 20 μl . Primer sequences and fragment sizes are listed in Table S1. The qPCR program was 50°C for 2 min, 95°C for 10 min, 40 cycles of 95°C for 15 s and 60°C for 1 min; and a final dissociation stage of 95°C for 15 s, 60°C for 1 min, and 95°C for 30 s. A previous experiment was performed to assess for primer efficiency with different sets of primers for each target gene. Primer efficiencies of the chosen sets are listed in the Table S1.

Low-Temperature Scanning Electron Microscopy

Leaf pieces were mounted on aluminum stubs with adhesive (Gurr[®], optimum cutting temperature control; BDH, Poole, UK), cryo-fixed in slush nitrogen (-196°C), cryo-transferred to a vacuum chamber at -180°C , and then fractured using a stainless steel spike. Once inside the microscope, the samples underwent superficial etching under vacuum (-90°C , 120 s, 2 kV), and then were overlaid with gold for observation and microanalysis. This freeze-fracture procedure leads to cell rupture only at

the fracture plane, whereas the general internal leaf structure is well-preserved. Fractured samples were observed at low temperature with a digital scanning electron microscope (Zeiss DSM 960, Oberkochen, Germany) using secondary and back-scattered electrons. Secondary electron images (1024 × 960 pixels) were obtained at 133 eV operating at a 35° take-off angle, an accelerating voltage of 15 kV, a working distance of 25 mm and a specimen current of 1–5 nA. Microscopy was run in the Institute of Agricultural Sciences-CSIC (ICA-CSIC), Madrid, Spain.

Results

Sugar beet plants showed Fe-deficiency symptoms 5 days after the treatment onset, with a marked yellowing of the younger leaves (Table S2). A freeze-fracture electron microscopy micrograph provided a representative image of a *B. vulgaris* leaf, with the apoplastic space surrounding mesophyll cells, as well as the epidermal cells and the minor vein tissues (Figure 1). The micrograph also shows the presence of plasmodesmata that communicate neighboring cells.

The apoplastic fluid collected from these leaves was assayed for c-mdh activity and only samples with contamination levels <3% (mean 1.72%, expressed on a total leaf activity basis) were used for 2-DE protein profiling (Table S2). Typical protein extraction yields ranged between 0.4 and 0.8 μg protein μL⁻¹ of apoplastic fluid (Table S2).

Protein Profiles of the Apoplastic Fluid

The protein profile of apoplast extracts from *B. vulgaris* leaves was studied by 2-DE IEF-SDS-PAGE electrophoresis.

Experimental conditions allowed for the separation of proteins within pI and MW ranges from 3.5 to 8 and from 18 to 106 kDa, respectively. Typical real scans of 2-DE gels obtained from apoplastic fluid protein extracts of Fe-sufficient (+Fe), Fe-deficient (-Fe), and Fe-resupplied Fe-deficient plants (-FeR) are shown in Figures 2A–C, respectively. The average number of detected spots (mean ± SD) was 210 ± 12, 216 ± 11, and 211 ± 20 in gels from plants grown in +Fe, -Fe, and -FeR conditions, respectively (Table S3 and Figure S1). The total number of spots consistently detected in the whole experiment (present in all four gels of at least one treatment) was 203. A composite averaged virtual map containing all consistent spots is shown in Figure 2D. All consistent spots were analyzed by MS, and proteins were unambiguously identified in 78% of the cases (158 spots) (Table S4 and Figure S1). A large percentage (97%) of identifications was achieved using the best custom reference repository. To identify UniProt entries, BLAST searches (*E*-values < 1e-30) of the unambiguously identified protein hits were run when needed. This approach revealed a high degree of redundancy in the identified protein species. When duplicates (same UniProt entry) were removed, the 158 identified proteins were reduced to 109 non-redundant proteins and this protein set was considered as the leaf apoplastic protein profile (Table 1). However, it should be noted that there may be still certain degree of redundancy left, since some hits correspond to the same protein description but from different plant species (Table 1).

The distribution of non-redundant proteins according to the biological process in the sugar beet leaf apoplast indicated that the major functional categories within the apoplastic proteome were C metabolism (25%; 27 protein species), stress and defense

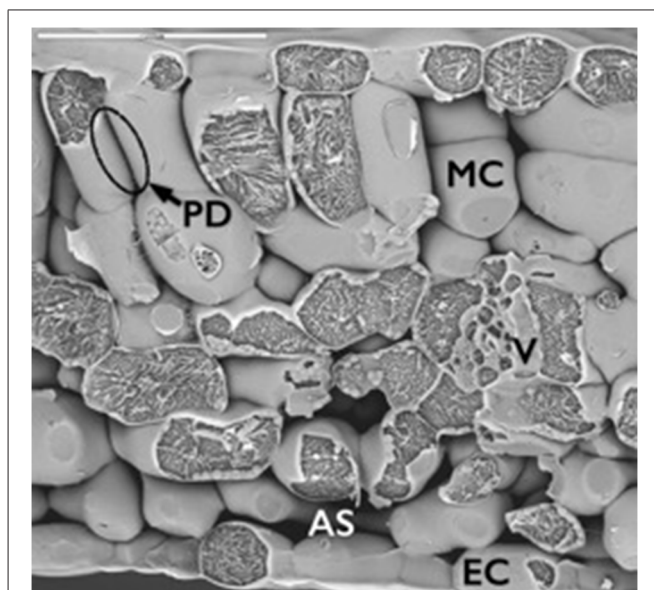


FIGURE 1 | Freeze-fracture low-temperature scanning electron micrograph of a transversal section from a *Beta vulgaris* leaf. This leaf transversal section gives three-dimensional information on the internal structure of the leaf. Apoplastic space (AS in white letters) surrounds mesophyll (MC) and epidermal cells (EC). The image also shows the presence of plasmodesmata (PD) that communicate neighboring mesophyll cells.

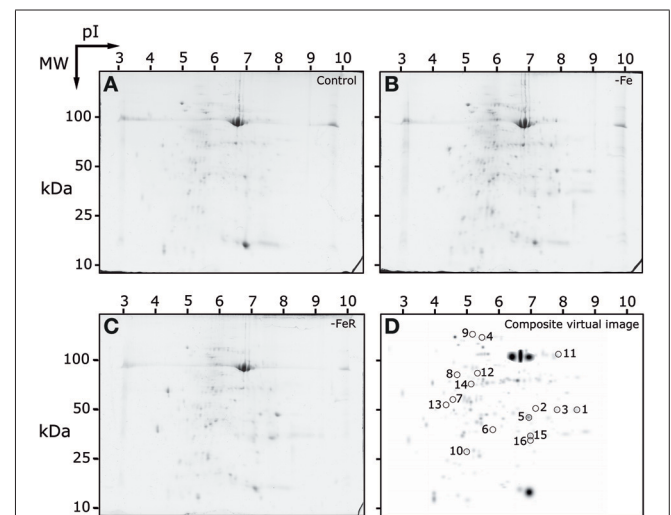


FIGURE 2 | 2-DE IEF-SDS PAGE protein profile maps of leaf apoplastic fluid extracts from sugar beet plants. Scans of typical gels from Fe-sufficient (+Fe), Fe-deficient (-Fe) and Fe-resupplied Fe-deficient (-FeR) plants are shown in (A–C), respectively. To facilitate visualization of the studied spots, a virtual composite image (D) was created containing all spots present in the real gels (A–C). In (D) spots whose intensities changed in relative abundance as a result of the treatments are circled and numbered as in Table 2.

TABLE 1 | Non-redundant proteome of the leaf apoplastic fluid of sugar beet plants.

Number of spots ^a	Protein description ^b	UniProt ^c	TargetP ^d	SecretomeP ^e	Go:Pf
PROTEIN METABOLISM (21)					
2	Proteasome subunit alpha type	D7T9I6, I6U5E4	–, M	–, nCS	Ubiquitin-dependent proteolysis
1	Proteasome subunit alpha type-5	Q9M4T8	–	–	Ubiquitin-dependent proteolysis
1	Proteasome subunit alpha type-6-like isoform X1	XP_004488480	–	–	Ubiquitin-dependent proteolysis
1	Proteasome subunit beta type-6	M4D453	–	nCS	Ubiquitin-dependent proteolysis
1	Proteasome subunit alpha type-7	XP_008393990	–	–	Ubiquitin-dependent proteolysis
1	Cysteine proteinase RD19a/like	I1LJ95	S	CS	Proteolysis
1	Cysteine protease	A5HIJ1	S	CS	Proteolysis
1	Aspartic protease	A0A067FW02	S	CS	Proteolysis
2	Serine carboxypeptidase	W9SXH8, B9SMP4	S, S	CS, CS	Proteolysis
2	Serine carboxypeptidase-like 20-like	XP_008235895	S	CS	Proteolysis
2	Unknown protein with peptidase domain	E0CQB3	–	nCS	Serine-type endopeptidase activity
1	Subtilisin-like protease-like	XP_006466502	S	CS	Serine-type peptidase activity
1	Chaperonin 20	A0A061GL19	C	–	Protein folding
3	Peptidyl-prolyl cis-trans isomerase	B9RN18, O49939	C, C	–, nCS	Protein folding
1	Rubisco subunit binding-protein alpha subunit	B9MZ75	C	–	Protein folding
1	Heat shock 70 protein	O22664	–	–	Protein folding
1	Predicted heat shock cognate 70 kDa protein 2-like	XP_004505872	–	–	Protein folding
1	Elongation factor Tu	A0A067FTF8	C	nCS	Translation
CARBON METABOLISM (27)					
4	Enolase	Q43130	–	nCS	Glycolytic process
4	Triosephosphate isomerase	B0LT90, K4FXE7, P48496	–, –, C	–, nCS, nCS	Glycolytic process
11	Fructose-bisphosphate aldolase	F1AHC9, O04975, Q6RSN7	C, –, –	nCS, nCS, –	Glycolytic process
1	2,3-Bisphosphoglycerate-independent phosphoglycerate mutase	Q42908	–	–	Glycolytic process
1	Phosphoglucomutase	P93262	–	–	Glucose metabolic process
3	Glyceraldehyde-3-phosphate dehydrogenase	A3FMH0	–	–	Glucose metabolic process
2	Ribose-5-phosphate isomerase	Q8RU73	C	nCS	PPS, non-oxidative branch
1	Ribulose-phosphate 3-epimerase	Q43157	C	nCS	Calvin cycle; PPS, oxidative branch
3	Transketolase	O20250, Q14K68	C, –	nCS, nCS	Calvin cycle; PPS, oxidative branch
1	Phosphoglycerate kinase	P29409	C	–	Calvin cycle, glycolytic process
1	Sedoheptulose-1,7-bisphosphatase	O20252	C	nCS	Calvin cycle
1	Phosphoribulokinase	P09559	C	–	Calvin cycle
6	Ribulose-1,5-bisphosphate carboxylase/oxygenase	Q08184, XP_004144069, P16032, A0A023ZPS4, Q6JXV6	C, C, C, –, –	nCS, –, nCS, nCS, nCS	Carbon fixation
3	23 kDa OEC protein	B0L802	–	–	Photosynthesis
5	Malate dehydrogenase, cytoplasmic	Q9SML8	–	nCS	Cellular carbohydrate metabolic process
5	Carbonic anhydrase	P16016, U5GK55	C, S	nCS, CS	One-carbon metabolic process
1	Oxaloacetase (<i>Dianthus caryophyllus</i>)	Q05957	–	–	Metabolic process

(Continued)

TABLE 1 | Continued

Number of spots ^a	Protein description ^b	UniProt ^c	TargetP ^d	SecretomeP ^e	Go:Pf ^f
STRESS AND DEFENSE (23)					
3	Osmotin-like protein	Q38745	S	CS	Defense response
4	Thaumatococcus-like protein	Q6PP01, A9ZMG1, A9ZMG0, XP_004297839	-, S, S, S	nCS, CS, CS, CS	Defense response
1	Abscisic acid stress ripening-related protein	A0A059SPX5	-	-	Response to stress
1	Protein IN2-1 homolog B-like	XP_003632205	C	nCS	Glutathione metabolic process
1	Uncharacterized protein with Bet_v_1_allergen domain	M0ZYA5	-	-	Defense response
1	Ascorbate peroxidase	Q94CF7	-	-	Response to oxidative stress
1	Monodehydroascorbate reductase	Q93YG1	S	CS	Response to oxidative stress
1	Peroxidase superfamily protein	XP_007014796	S	CS	Response to oxidative stress
1	Peroxidase	P93547	S	CS	Response to oxidative stress
3	Peroxioredoxin	H6VND7	C	nCS	Cell redox homeostasis
1	Type II peroxiredoxin	I0CC96	M	nCS	Cell redox homeostasis
1	Cu/Zn superoxide dismutase	H9BQP8	C	CS	Superoxide metabolic process
6	Lactoylglutathione lyase	M0ZHD0, D2D330, Q8W593, GI:697188226, GI:697141977	C, -, C, -, C	nCS, -, nCS, -, -	Methylglyoxal catabolic process to D-lactate
2	Lactoylglutathione lyase isoform X2	GI:694332574, XP_008385524	-, -	-, -	Methylglyoxal catabolic process to D-lactate
1	Predicted isoflavone reductase homolog	XP_008377292	S	CS	Oxidation-reduction process
POLYSACCHARIDE METABOLISM (10)					
2	3-Glucanase family protein	B9GI31	S	CS	Carbohydrate metabolic process
2	Acidic endochitinase SP2	P42820	S	CS	Polysaccharide catabolic process
1	Acidic endochitinase SE2	P36910	S	CS	Polysaccharide catabolic process
4	Chitinase	Q8LST3	S	CS	Carbohydrate metabolic process
2	Beta-xylosidase/alpha-L-arabinofuranosidase	XP_008218886	S	CS	Xylan catabolic process
1	UDP-glucuronic acid decarboxylase 1	W9R277	C	nCS	UDP-D-xylose biosynthetic process
2	Beta-fructofuranosidase	Q8VXS6, S49256	-, -	nCS, nCS	Carbohydrate metabolic process
1	Uncharacterized protein with hydrolase domain	V4SY44	M	CS	Carbohydrate metabolic process
1	Unknown protein with hydrolase domain	A9PG55	-	nCS	Mannose metabolic process
AMINO ACID METABOLISM (7)					
3	Serine hydroxymethyltransferase	XP_007034218, XP_007034219	-, -	-, -	L-serine metabolism
1	Serine transhydroxymethyltransferase	P50433	M	-	L-serine metabolism
1	Aminomethyltransferase	P93256	M	nCS	Glycine catabolism
3	Glutamine synthetase	Q9AWA8, Q9AXD1	C, -	-, -	Glutamine biosynthesis
2	Aspartate aminotransferase	B9HAW0	C	nCS	Cellular amino acid metabolic process
LIPID METABOLISM (3)					
1	3-Hydroxybutyryl-CoA dehydratase	B9RPB0	M	nCS	Enoyl-CoA hydratase activity
1	Uncharacterized protein with lipase domain	U5FE87	S	CS	Lipid metabolic process
1	Uncharacterized protein with lipase domain	D7TJU3	S	CS	Lipid metabolic process

(Continued)

TABLE 1 | Continued

Number of spots ^a	Protein description ^b	UniProt ^c	TargetP ^d	SecretomeP ^e	Go:Pf ^f
OTHER (9)					
1	Ferredoxin-NADP reductase	B9SB31	C	nCS	Oxidation-reduction process
3	Alcohol dehydrogenase	B9SHB0	C	–	Oxidation-reduction process
1	Flavoprotein WrbA-like	XP_004294313	–	–	Oxidation-reduction process
2	Acylypyruvase FAHD1	XP_004508199	–	–	Hydrolase activity
1	Cytosolic ATP sulfurylase	G9B7N0	–	–	Sulfate assimilation
1	Nucleoside diphosphate kinase 2	Q01402	C	nCS	Nucleotide metabolic process
1	Thiamine thiazole synthase	XP_008244366	C	nCS	Thiamine biosynthetic process
1	Uncharacterized germin protein	I3SGS4	S	CS	Nutrient reservoir activity
1	Soluble inorganic pyrophosphatase 1	A0A061E4X1	M	nCS	Pyrophosphatase activity
UNKNOWN FUNCTION (9)					
1	Putative protein (<i>Hordeum vulgare</i>)	F2EID0	–	–	Nucleotide binding
4	Uncharacterized protein (<i>Vitis vinifera</i>)	D7SXW6	S	CS	
1	Uncharacterized protein (<i>Jatropha curcas</i>)	A0A067KSH6	M	nCS	
1	Uncharacterized protein (<i>Jatropha curcas</i>)	A0A067KHD5	–	nCS	
1	Jasmonate-induced protein (<i>Atriplex canescens</i>)	P42764	–	nCS	
1	CSP41A protein	E5KGE2	–	–	Cellular metabolic process
1	Hypothetical protein CICLE_v10029208mg (<i>Citrus clementina</i>)	V4SBG5	S	CS	
2	No blast result				
NO IDENTIFIED					
45					

^aNumber of spots with the same protein description.

^bProtein description.

^cUniProt entries sharing same protein description.

^dTargetP algorithm predictions: C, M, S, and – indicate chloroplast, mitochondrion, secretory pathway and any other location, respectively.

^eSecretomeP algorithm predictions: CS, nCS and – indicate classical secreted, non-classical secreted, and non-secreted proteins, respectively.

^fDescription of the GO: P (biological process) term.

(21%; 23 proteins), and protein related processes (19%; 21 proteins), followed by cell wall related processes (9%, 10 proteins) (Table 1, Figure 3A).

From the non-redundant leaf apoplastic proteins, 26% (28 protein species) were predicted to have a signal peptide sequence using the TargetP or SecretomeP softwares, whereas SecretomeP revealed that 38% (41 proteins) were assigned to non-classical secreted proteins lacking a signal peptide (Table 1, Figure 3B).

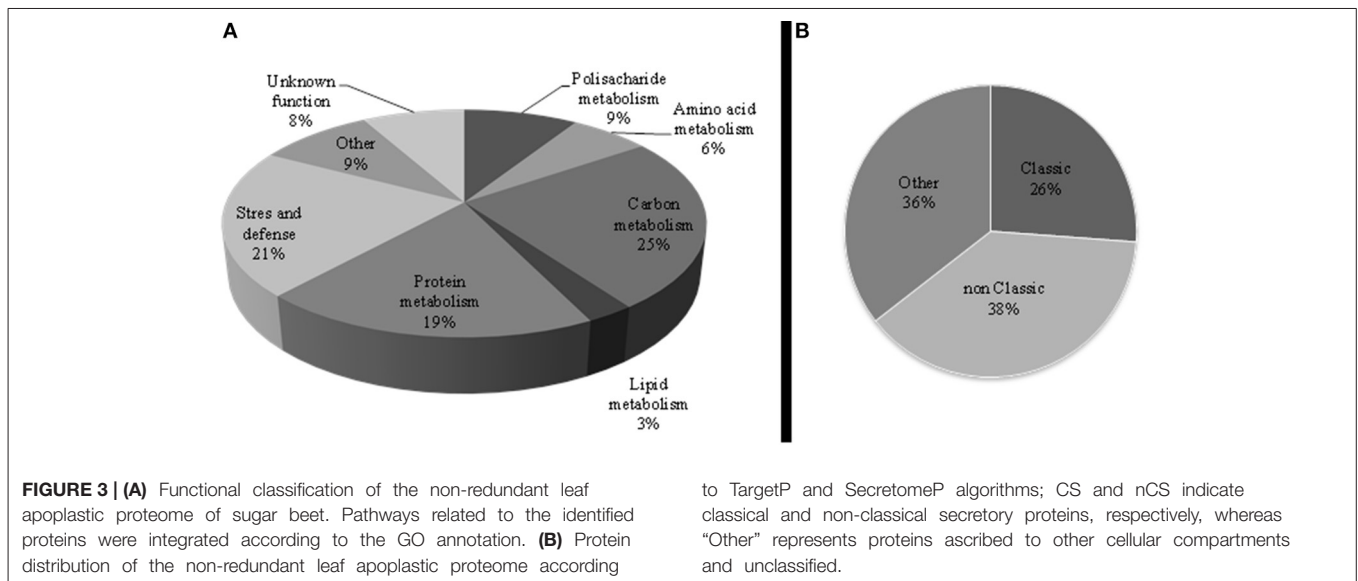
Effect of Fe-Deficiency and Fe Resupply on the Leaf Apoplastic Fluid Protein Profile

The statistical analysis ($p < 0.05$; t -Student) of averaged 2-DE maps indicated that 8% (16 spots) of the total number of consistent spots changed significantly and >2-fold in relative abundance in the whole experiment (spots labeled 1–16 in Figure 2D). Among them, 88% of the spots (14) matched reliably to known proteins and were identified by database searches (1–14, Figure 2D). Their metabolic functions were assessed manually by GO annotation and identified proteins were classified into five functional categories: cell wall related processes (4 spots, 2 proteins), protein metabolism (4 proteins), and defense, amino

acid and C-related pathways, with two proteins each (Table 2). The principal component analysis of differentially accumulated spots showed a good separation between treatments, with the first and second components explaining approximately 48 and 38% of the variation, respectively (Figure 4).

When the protein profile of -Fe samples was compared to that of the +Fe samples, only five spots changed in relative abundance. Four of them increased, including three spots (spots 1–3) identified as chitinase and one (spot 9) identified as a thaumatin-like protein. Only one spot (spot 13) decreased as a result of Fe deficiency and it was identified as carbonic anhydrase (Figure 2D, Table 2).

In the comparison of -FeR vs. +Fe, eight spots changed in relative abundance, four of them increased whereas the other four decreased (Figure 2D, Table 2). Two of the spots increasing in relative abundance were identified as chitinase and thaumatin (spots 2 and 9, respectively) whereas the other two could not be identified (spots 15 and 16). The spots decreasing in relative abundance were identified as a cysteine proteinase RD19-like protein (spot 5), a peptidyl-prolyl *cis-trans* isomerase (spots 6, 7) and a serine hydroxymethyltransferase (spot 11) (Table 2).



When the -FeR samples were compared to the -Fe ones, six spots changed in relative abundance (**Table 2**). Among them, one spot was detected *de novo* (spot 14) and identified as the 23 kDa OEC protein and a second one (spot 15) could not be identified. Four spots showed significant decreases in relative abundance (**Table 2, Figure 2D**), and they were identified as β -xylosidase/alpha-L-arabinofuranosidase (spot 4), a cytosolic heat shock 70 protein (spot 8), lactoylglutathione lyase (spot 10) and glutamine synthetase (spot 12).

Relative Transcript Abundance of Target Genes

The chitinase and thaumatin-like 1 proteins identified in spots 1 and 9 (**Table 2** and Table S4, **Figure 2**), respectively, showed the highest increases in relative abundance as a result of Fe-deficiency and were selected to study transcript abundances using q-PCR. Sequences containing the peptides matched during protein identification, KDHBv_S14175_58500.t1 for chitinase and BQ584258 for the thaumatin-like 1 protein, were selected to design primers for specific amplification of target genes (Table S1). In Fe-deficient leaves, the relative abundances of chitinase and thaumatin-like 1 protein transcripts increased 3- and 2-fold, respectively, when compared to controls (**Figure 5**), whereas upon Fe resupply the relative abundance of chitinase transcript was higher and that of thaumatin-like 1 protein was not significantly different at $p < 0.05$ (**Figure 5**). When compared to the Fe-deficient controls, changes in transcript abundances upon Fe-resupply were not statistically significant at $p < 0.05$ (**Figure 5**).

Discussion

Leaf Apoplastic Protein Profile

The 2-DE proteomic approach allowed us to resolve 203 spots, with 158 of them (78%) being identified and 109 accounting for non-redundant proteins. These results are similar to those reported for gel-based leaf apoplastic proteome studies in other

plant species, which ranged between 93 and 470 spots, with an average of 200 spots in most of the studies (**Table 3** and references therein). Functional classification of the non-redundant leaf apoplastic proteins of sugar beet indicates that stress and defense, protein metabolism, cell wall and C metabolism account for approximately 75% of the identified proteome (**Figure 3A**).

Stress and defense related proteins accounted for 21% of the non-redundant sugar beet apoplastic proteome. Similar to what has been reported in other plant species (references in **Table 3**), proteins identified were peroxidases, osmotin-like, thaumatin-like, and pathogenesis-related proteins. Our results also indicate the presence in the leaf apoplast of enzymes participating in defense against oxidative stress (two peroxidases, CuZnSOD and two enzymes from the ascorbate-glutathione cycle: ascorbate peroxidase and monodehydroascorbate reductase) and in the detoxification of methylglyoxal (two UniProt entries described as glyoxalase I). These proteins have also been found in the leaf apoplast from poplar (Pechanova et al., 2010) and are also present in fluids from the vascular tissue (Lattanzio et al., 2013; Lucas et al., 2013). The presence of this wide spectrum of defense proteins in non-stressed plants has been attributed to a pre-formed defense that creates a hostile environment for pathogens (Pechanova et al., 2010; Delaunoy et al., 2013).

The contribution of protein metabolism-related proteins to the sugar beet apoplastic proteome (19%, with 14 of the 21 UniProt entries being proteases) is within the range reported in other studies using grapevine, Arabidopsis, and rice (16–20%; Floerl et al., 2012; Delaunoy et al., 2013; Kim et al., 2013), but higher than percentages described for other plant species, which range from 6 to 10% (Boudart et al., 2005; Goulet et al., 2010; Pechanova et al., 2010). The presence of such a high number of proteolysis-related proteins in the apoplast has been proposed to be species-dependent (Delaunoy et al., 2013). Subtilisin-like, serine-carboxypeptidases, and aspartic proteases found in this study have been consistently described in the apoplast of several plant species (Goulet et al., 2010; Floerl et al., 2012;

TABLE 2 | Spots showing differences in relative abundance (Student *t*-test *p* < 0.05) as a result of Fe deficiency and Fe resupply.

Spot number in Figure 1 ^a	SSP number ^b	–Fe vs. +Fe ^c	–FeR vs. +Fe ^d	–FeR vs. –Fe ^e	Protein ^f	Plant Species ^g	Uniprot ^h	GO:Pi	SecretomePi ⁱ
POLYSACCHARIDE CATABOLISM									
1	9403	new	<i>new</i>	–8.1	Chitinase from <i>Phytolacca americana</i>	<i>Beta vulgaris</i>	Q8LST3	Carbohydrate metabolic process	CS
2	7404	8.7	5.3	–1.6	Chitinase from <i>Phytolacca americana</i>	<i>Beta vulgaris</i>	Q8LST3	Carbohydrate metabolic process	CS
3	8401	4.2	3.0	–1.4	Chitinase from <i>Phytolacca americana</i>	<i>Beta vulgaris</i>	Q8LST3	Carbohydrate metabolic process	CS
4	3805	1.4	–3.6	–5.0	Beta-xylosidase/alpha-L-arabinofuranosidase from <i>Prunus mume</i>	<i>Beta vulgaris</i>	XP_008218886*	Xylan catabolic process	CS
PROTEIN RELATED									
5	1402	–1.8	–6.5	–3.7	Cysteine proteinase RD19a-like from <i>Glycine max</i>	<i>Beta vulgaris</i>	I1LJ95	Proteolysis	CS
6	2203	–1.1	–3.6	–3.2	Peptidyl-prolyl cis-trans isomerase from <i>Ricinus communis</i>	<i>Beta vulgaris</i>	B9RN18	Protein folding	nCS
7	1602	–3.1	–7.9	–2.6	Peptidyl-prolyl cis-trans isomerase from <i>Spinacia oleracea</i>	<i>Beta vulgaris</i>	O49939	Protein folding	nCS
8	2902	1.2	–2.1	–2.4	Cytosolic heat shock 70 protein from <i>Spinacia oleracea</i>	<i>Beta vulgaris</i>	O22664	Protein folding	–
DEFENSE									
9	1404	19.5	11.5	–1.7	Thaumatococin-like protein 1 from <i>Fragaria vesca</i>	<i>Beta vulgaris</i>	XP_004297839*	Defense response	CS
10	2503	1.2	–2.0	–2.3	Lactoylglutathione lyase from <i>Gossypium hirsutum</i>	<i>Beta vulgaris</i>	D2D330	Methylglyoxal catabolic process to D-lactate	nCS
AMINO ACID METABOLISM									
11	8710	–1.7	–5.0	–3.0	Serine hydroxymethyltransferase from <i>Theobroma cacao</i>	<i>Beta vulgaris</i>	XP_007034218*	L-serine metabolic process	–
12	2610	2.3	–6.3	–14.2	Glutamine synthetase	<i>Beta vulgaris</i>	Q9AXD1	Glutamine biosynthesis	–
CARBON METABOLISM									
13	7302	–2.2	–1.8	1.2	Carbonic anhydrase from <i>Spinacia oleracea</i>	<i>Beta vulgaris</i>	P16016	One-carbon metabolic process	nCS
14	4307	ND	–12.2	new	23 kDa OEC protein from <i>Salicornia veneta</i>	<i>Beta vulgaris</i>	B0L802	Photosynthesis	–
NO IDENTIFIED									
15	7202	1.5	6.1	4.1					
16	7204	4.7	2.4	–2.0					

^aSpot number as in Figure 1.^bSpot number as in Table S3.^{c–e}Fold change in the Fe-deficient vs. Fe sufficient, Fe resupplied vs. Fe-sufficient and Fe-resupplied vs. Fe-deficient comparisons, respectively, values in bold indicate significant changes and when the ratios were lower than one the inverse was taken and the sign changed.^fProtein description.^gPlant Species.^hUniprot entry (denotes protein entry in UniParc).ⁱGO:Pi term description.ⁱSecretomeP algorithm predictions: CS, nCS and – indicate classical secreted, non-classical secreted and non-secreted proteins, respectively.

Delaunoy et al., 2013). In addition, our results indicate that sugar beet apoplast also contains several subunits of the proteasome (six UniProt entries), which is involved in the ubiquitin dependent degradation of damaged and miss-folded proteins

(Kurepa and Smalle, 2008). These apoplastic proteases may play a role in plant defense against pathogens and also in signaling (Van Der Hoorn and Jones, 2004; Xia et al., 2004; Pearce et al., 2010).

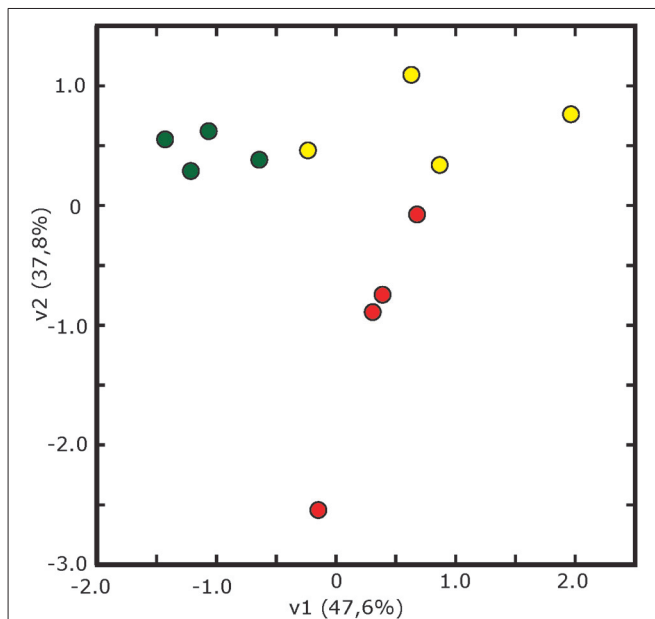


FIGURE 4 | Multivariate statistical analysis (Principal Component Analysis, PCA) of 2-DE gels. Score scatter PCA plot of component 1 vs. component 2 after analysis of spots showing differences in relative abundance from leaf apoplastic fluid of sugar beet plants grown in Fe-sufficient (green circles), Fe-deficient (yellow circles) and Fe-resupplied Fe-deficient (red circles) conditions.

The cell wall related category accounted for 9% (10 proteins) of the sugar beet leaf proteome and included nine glycoside hydrolases. Glycoside hydrolases modify cell walls by metabolizing carbohydrate compounds from plant cell polysaccharides and by interacting with hemicellulases and pectic enzymes (Numan and Bhosle, 2006; Minic, 2008). The percentage of cell wall related proteins found in sugar beet is similar to those reported in grapevine and tobacco but lower than those found in rice, poplar or maize (Table 3). On the other hand, the percentage of proteins participating in C-related processes in the leaf apoplast of sugar beet was slightly higher (25%, 27 proteins) than those reported in other plant species (Table 3 and references therein). However, these values vary depending on the functional classification of certain proteins, such as peroxidases that are included in defense or cell wall depending on the study, and on the consideration of carbohydrate metabolism and cell wall as one or two functional categories.

The relatively high percentage of C-related proteins found in the sugar beet leaf proteome may have several causes. First, a large number of the spots identified as proteins participating in C metabolism have a low spot intensity and therefore they are over-represented in the functional categorization based on protein number. Second, the sugar beet apoplastic proteome was obtained by direct leaf centrifugation, whereas most of the proteomes from other plant species were obtained using leaf vacuum infiltration followed by centrifugation (Table 3 and references therein); this later technique may be somewhat better at preventing leakage of proteins from the cytoplasm (Lohaus

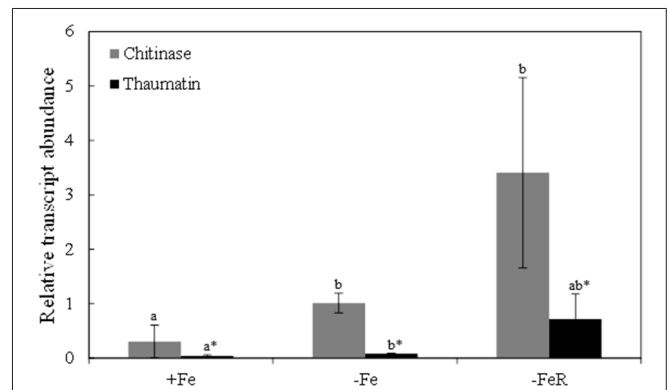


FIGURE 5 | Relative abundances of chitinase and thaumatin-like 1 transcripts measured in leaves by qRT-PCR using tubulin as housekeeper gene. Sequences containing the peptides matched during protein identification, KDHBv_S14175_58500.t1 for chitinase and BQ584258 for the thaumatin-like 1, were selected to design primers for specific amplification (Table S1). Data are means \pm SD of two experiments with four biological and two technical replicates per treatment in each experiment. Different letters indicate statistically significant differences at $p < 0.05$.

et al., 2001; Witzel et al., 2011). Interestingly, the percentage of C-related proteins in the stem apoplast of poplar (18%) as well as the identity (TCA and glycolysis-related) (Pechanova et al., 2010), are similar to those found in sugar beet (25%). This comparison might suggest that the sugar beet apoplastic fluid obtained by direct centrifugation of the leaves could have a high contribution of the fluid contained in the xylem sap vessels of the main vein of the leaf.

The presence of cytoplasmic contamination in our samples was always lower than 3%, with an average value of 1.5%, as assessed by the activity of *c-mdh* (Table S2). However, *in silico* analysis of the non-redundant proteome using the TargetP and the Secretome P algorithms (for classical and non-classical secretory proteins) predicted 26% (28 proteins) and 38% (41 proteins) of the non-redundant proteome as classical and non-classical secretory proteins, respectively, whereas 36% of the proteins were predicted to be non-secretory (Table 1, Figure 3B). This percentage (64%) of secretory proteins is within the range of those reported in the leaf apoplast proteome of other plant species (from 50% in Arabidopsis to 80% in grapevine and poplar; Casasoli et al., 2008; Pechanova et al., 2010; Delaunois et al., 2013). The fact that our samples contain a relative large number of proteins tagged as non-secretory is not surprising, since the *c-mdh* assay indicates that up to 3% of the leaf cells could have delivered cytosolic components into the isolated apoplastic fluid. Furthermore, the release of cytosolic components may be in part associated to the rupture of the plasmodesmata that exist in these leaves (Figure 1), even if mesophyll cells remain intact. On the other hand, RuBisCO was identified in six spots of the total 203 of the leaf apoplastic proteome map (Table S4). In addition there were 10 more spots whose identification yielded proteins related to the Calvin cycle and are, most likely, plastid located (Table 1). Therefore, we could assume that at least 16 spots (approximately 8% of the total) are probably a result of cell leakage. These results may suggest

TABLE 3 | Summary of proteomic studies on leaf apoplast.

References	Plant specie	Technique	Leaf material	Study	Separation	Number of spots	Analysis	Changes	Functional classification in control
Fecht-Christoffers et al., 2003	<i>Vigna unguiculata</i>	VIC-(water)	Whole leaf	Mn toxicity	18 cm 18 cm	3–10 N BN-PAGE	Not reported	10	Not reported
Boudart et al., 2005	<i>Arabidopsis thaliana</i>	VIC-(0.3 M mannitol)	Whole rosette leaves	Mapping	7 cm	4–7	93 identified	–	32 % cell wall modifying proteins, 21 % defense-related, 20% proteins with interacting domains, 11 % proteinases
Dani et al., 2005	<i>Nicotiana tabacum</i>	VIC-(1 M NaCl, 0.2 M CaCl ₂ , 2 M LiCl or 0.3 M CDTA)	Whole rosette leaves		Sepharose fractioning followed by 1DE	87		–	
Dani et al., 2005	<i>Nicotiana tabacum</i>	VIC- (50 mM phosphate buffer, 200mM NaCl, pH 7)	1-2 cm 2 leaf strips	Salt stress	7 cm	3–10	150	20	Not reported
Soares et al., 2007	<i>Medicago truncatula</i>	VIC-(15 mM sodium acetate buffer, pH 4.5)	Leaf pices	Mapping	Not specified	3–10 NL	220	–	38% defense, 58 % unknown
Casasoli et al., 2008	<i>Arabidopsis thaliana</i>	VIC-(25 mM Tris-HCl pH7.4, 50mM EDTA, 150mM MgCl ₂)	Seedlings	Oligogalacturonides	DIGE-13 cm	3–10	180–220	16	30% secretory pathway, 20% chloroplast, 14% cell wall
Floerl et al., 2008	<i>Brassica napus</i>	VIC-(100 mM KCl, 0.01 % Triton)	Leaf without midrib	Fungus infection	18 cm	3–10	170	12	Chitinases, proteases, peroxidases, glucanases, germin, cell wall modification
Soares et al., 2009	<i>Medicago truncatula</i>	VIC-(water)	Leaf-halves	Wounding	Not specified	3–10 NL	110	28	Defense or unknown
Pechanova et al., 2010	<i>Populus deltoides</i>	Pressure chamber	Whole leaf	Mapping	24 cm	3–10 NL	84	–	25% cell wall, 24% stress-defense, 12% proteolysis, 8% cell wall, 4% carbohydrate
					2D-LC		106	–	

(Continued)

TABLE 3 | Continued

References	Plant specie	Technique	Leaf material	Study	Separation	Number of spots	Analysis	Changes	Functional classification in control
Goulet et al., 2010	<i>Nicotiana benthamiana</i>	VIC (10 mM MES, pH 5.8)	Whole leaf	Agrobacterium infection	3–10 NL	Ca. 200	91 analyzed and 73 identified	44	29% defense, 15% cell wall, 6% proteases
Witzel et al., 2011	<i>Zea mays</i>	VIC-(water/ 100mM sodium phosphate buffer/25 mM Tris-HCl/ 100 mM sorbitol/20 mM ascorbic acid and 20 mM CaCl ₂ / 50 mM NaCl)	5.5 cm leaf segments	Infiltration technique	3–10	171/107/131/133/133/114 328 total	67 identified as apoplastic proteins by in silico (20%)	–	58% Carbohydrate metabolism and cell wall, 22% defense, 10% protein transporting function, 27% cytosol proteins, 13% chloroplast proteins
Floerl et al., 2012	<i>Arabidopsis thaliana</i>	VIC (100 mM KCl, 0.005% Triton X-100)	Whole leaf	Fungus infection	3–10	217	45 analyzed and identified	7	25% carbohydrate metabolism, 18% proteases, 21% oxidoreductases
Shenton et al., 2012	<i>Oryza sativa</i>	VIC-(60 mM Na-P buffer pH7.5, 600mM NaCl, 0.01% Tween-20, 0.1% β-mercapto ethanol)	Whole leaf	Fungus infection	3–11 NL	Not reported	–	–	Not reported
Delaunais et al., 2013	<i>Vitis vinifera</i>	VIC-(150 mM Tris-HCl, pH 8.5, 6mM CHAPS)	1 cm 2 leaf cuts	Mapping	3–10 NL	306	177 analyzed and 89 identified	–	On protein number basis: 28% defense, 18% cell wall / on spot volume basis: 51% defense, 16% proteases, 12% cell wall
Kim et al., 2013	<i>Oryza sativa</i>	CA-VIC (200 mM CaCl ₂ , 5mM Na-acetate, pH 4.3)	5 cm leaf cuts	Fungus infection	4–7	27	–	12	21% carbohydrate metabolism, 20 % protein metabolism, 30 % defense, 12 % energy pathway
					MudPIT	283			

(Continued)

TABLE 3 | Continued

References	Plant specie	Technique	Leaf material	Study	Separation	Number of spots	Analysis	Changes	Functional classification in control
Petriccione et al., 2014	<i>Actinidia deliciosa</i>	VIC-(100mM Tris-HCl, pH 7.5, 10 mM KCl, 1mM phenylmethanesulfonyl fluoride)	Leaf without midrib	Pseudomonas infection	7 cm	3-10	ca. 220	60	Not reported
Kim et al., 2014	<i>Oryza sativa</i>	CA-VIC-(200 mM CaCl ₂ , 5 mM Na-acetate, pH 4.3)	5 cm leaf cuts	Fungus infection	Shotgun	470	174 secreted proteins by in silico analyses		Not reported

VIC stands for vacuum infiltration followed by centrifugation.

that the real contamination by cell rupture is likely to be higher than that estimated by the use of *c-mdh* as a contamination marker.

Changes Induced by Fe Deficiency in the Leaf Apoplastic Proteome

The largest part of the changes caused by Fe-deficiency and Fe-resupply corresponded to proteins tagged as secretory proteins (10 spots), probably corresponding to true components of the apoplast. Changes also occurred in a relatively small number (four) of the apoplastic fluid proteins tagged as non-secretory ones, and possibly associated to cell or plasmodesmata rupture (these are marked by * in the following paragraphs).

Iron-deficiency caused changes in the relative abundance of five spots (2.5% of the consistent spots of the leaf apoplast proteome), suggesting that protein homeostasis in the leaf apoplast fluid is well-maintained upon Fe shortage. This number of changes is markedly low when compared to those induced by Fe deficiency in other proteomes, including those of roots and thylakoids of sugar beet plants (44 and 53%, respectively; Andaluz et al., 2006; Rellán-Álvarez et al., 2010) and falls within the lower range of the number of changes caused by other abiotic stresses in the leaf apoplast (Table 3; Dani et al., 2005; Casasoli et al., 2008).

Three spots identified as chitinase increased in relative abundance as a result of Fe-deficiency (spots 1–3; Figure 2, Table 2). These three spots had the same molecular weight and different pIs (8.2, 7.1, and 7.6), indicating that Fe-deficiency alters the isoform pattern of this enzyme, with one of the isoforms identified *de novo* in Fe-deficient samples. Chitinases are hydrolytic enzymes that break down glycosidic bonds, removing xylosyl residues of xyloglucan oligosaccharides in the cell wall (Sampedro et al., 2001). Therefore, these increases in chitinase suggest the existence of Fe deficiency-induced cell wall modifications. This is in agreement with the changes elicited by Fe deficiency in leaf morphology, which include reduction of xylem vessel size (Fernández et al., 2008; Eichert et al., 2010). Furthermore, changes in lignification have been reported in roots of Fe-deficient pear and quince cultivars (Donnini et al., 2009) and cell wall related proteins commonly show changes in abundance in proteomic studies of Fe deficient plants (see López-Millán et al., 2013 for a review).

A spot identified as a thaumatin-like protein 1 (spot 9) also increased in relative abundance as a result of Fe-deficiency. Thaumathins are pathogenesis-related (PR) proteins from the PR5 subfamily, which are induced by biotic and abiotic stresses. Some members of PR5 subfamily have been described to play distinctive roles in the defense system that protects against high-salt stress or osmotic imbalance (Tachi et al., 2009), which is likely to occur in the Fe-deficiency treatment in the presence of CaCO₃. A PR5b protein also showed increases in abundance in roots and stems of Fe-deficient *M. truncatula* plants grown in the presence of CaCO₃ (Rodríguez-Celma et al., 2011), suggesting that thaumathins are ubiquitously up-regulated by Fe deficiency. Interestingly, both chitinase and the thaumatin-like 1 protein were also affected in the leaf proteome of cowpea submitted to Mn toxicity (Fecht-Christoffers et al., 2003).

Only one protein, identified as carbonic anhydrase (CA; spot 13), decreased as a result of Fe deficiency. Carbonic anhydrase interconverts CO₂ and bicarbonate to maintain the acid-base balance. A decrease in CA activity could be attributed to the presence of bicarbonate in the nutrient solution that may reach the leaf apoplast *via* xylem (Nikolic and Römheld, 2007). Although some mammalian CA isoforms are extra-cellular and have been described in saliva and milk (Karhumaa et al., 2001; Leinonen et al., 2001), and CA is classified as a non-classical secretory protein by SecretomeP, plant isoforms are distinct from an evolutionary standpoint and have been mainly localized in the chloroplast or the cytosol.

Changes Induced by Fe Resupply in the Leaf Apoplastic Proteome

Iron resupply to Fe deficient plants caused significant changes in the relative abundance of 13 spots when compared to either Fe-sufficient or Fe-deficient plants. These spots can be roughly classified into two major groups. The largest group (seven spots) was composed by those spots increasing in relative abundance (significantly or not) with Fe-deficiency and decreasing significantly with Fe resupply when compared either with the control or with Fe-deficient samples. This group contained two cell wall related proteins [chitinase (spot 2), and β -xylosidase (spot 4)], three stress-related proteins [a heat shock 70 protein (spot 8*), thaumatin-like 1 protein (spot 9), glyoxalase I (spot 10)], glutamine synthase (spot 12*) and the unidentified spot 16. These results indicate that Fe resupply causes changes in the short-term (within 24 h) in cell wall and stress-related processes of the Fe-resupplied plants toward values found in the Fe-sufficient controls. One more protein (spot 14*, the 23 kDa OEC protein, which nuclear-encoded and synthesized in the cytosol) was also responsive to short term Fe-resupply but followed a different trend, not-detected in Fe-deficient samples but detected upon Fe-resupply. This likely reflects transitory increases in the cytosolic levels of this protein upon short term Fe-resupply, which are necessary for the slight recovery of the photosynthetic system at this resupply stage (Larbi et al., 2004).

On the other hand, a second group of four spots (spots 5–7 and 11*) decreased in relative abundance with Fe deficiency (although not significantly) and decreased significantly upon Fe-resupply when compared either with controls or Fe-deficient samples. This group included two proteins identified as

protein-metabolism related [a cysteine protease (spot 5), a peptidyl-prolyl *cis-trans* isomerase (spots 6,7)] and a serine hydroxymethyltransferase (spot 11*). One more spot (spot 15, unidentified protein) followed the opposite behavior (increased). This group of proteins can be classified as not responsive to short term Fe-resupply, since they may require a time longer than 24 h to reset to control values after resupply.

Concluding Remarks

In summary, this study provides information on the composition of the apoplast proteome in *B. vulgaris* leaves, which appears to be quite similar to that of other previously studied plant species. The study shows that Fe deficiency and Fe resupply cause significant changes in a limited number of proteins in the leaf apoplast, and none of them is expected to play a significant role in metal homeostasis. This is in contrast with the intense changes previously found in the concentrations of metabolites (e.g., carboxylates) that could interact with metals in the same compartment. Data found contribute toward the understanding of metal homeostasis, and in particular on the still poorly known mechanisms of Fe acquisition by plant mesophyll cells. Results presented here open an interesting line of work regarding possible modifications of cell wall that ultimately may affect permeability or transport of Fe across the plasma membrane.

Acknowledgments

Work supported by the Spanish Ministry of Science and Competitiveness (MINECO; projects AGL2012-31988 and AGL2013-42175-R (co-financed with FEDER), and the Aragón Government (group A03). LCL, EGC, GL, and SV were supported by FPI-MINECO, I3P-CSIC and FPI-MINECO predoctoral contracts and a JAE-CSIC postdoctoral contract (co-financed by the European Social Fund), respectively. This paper is dedicated to the memory of Mr. Fernando Pinto (ICA-CSIC), electron microscopy expert.

Supplementary Material

The Supplementary Material for this article can be found online at: <http://www.frontiersin.org/journal/10.3389/fpls.2015.00145/abstract>

Figure S1 | Virtual composite image containing all consistent spots present in the real gels. Numbers are as in Table S4 (SSP).

References

- Abadía, J., Álvarez-Fernández, A., Rombolá, A. D., Sanz, M., Tagliavini, M., and Abadía, A. (2004). Technologies for the diagnosis and remediation of Fe deficiency. *Soil Sci. Plant Nutr.* 50, 965–971. Available online at: <http://ci.nii.ac.jp/naid/10014190869/en/>
- Abadía, J., Vázquez, S., Rellán-Álvarez, R., El-Jendoubi, H., Abadía, A., Álvarez-Fernández, A., et al. (2011). Towards a knowledge-based correction of iron chlorosis. *Plant Physiol. Biochem.* 49, 471–482. doi: 10.1016/j.plaphy.2011.01.026
- Álvarez-Fernández, A., Abadía, J., and Abadía, A. (2006). “Iron nutrition in plants and rhizospheric microorganisms,” in *Iron Deficiency, Fruit Yield and Fruit Quality*, eds L. L. Barton and J. Abadía (Dordrecht: Springer), 85–101.
- Andaluz, S., López-Millán, A.-F., De Las Rivas, J., Aro, E.-M., Abadía, J., and Abadía, A. (2006). Proteomic profiles of thylakoid membranes and changes in response to iron deficiency. *Photosynth. Res.* 89, 141–155. doi: 10.1007/s11220-006-9092-6
- Bendtsen, J. D. V., Jensen, L. J., Blom, N., Von Heijne, G., and Brunak, S. R. (2004). Feature-based prediction of non-classical and leaderless protein secretion. *Protein Eng. Des. Sel.* 17, 349–356. doi: 10.1093/protein/gzh037

- Bendtsen, J., Kiemer, L., Fausboll, A., and Brunak, S. (2005). Non-classical protein secretion in bacteria. *BMC Microbiol.* 5:58. doi: 10.1186/1471-2180-5-58
- Boudart, G., Jamet, E., Rossignol, M., Lafitte, C., Borderies, G., Jauneau, A., et al. (2005). Cell wall proteins in apoplastic fluids of *Arabidopsis thaliana* rosettes: identification by mass spectrometry and bioinformatics. *Proteomics* 5, 212–221. doi: 10.1002/pmic.200400882
- Brune, A., Urbach, W., and Dietz, K. J. (1994). Compartmentation and transport of zinc in barley primary leaves as basic mechanisms involved in zinc tolerance. *Plant Cell Environ.* 17, 153–162. doi: 10.1111/j.1365-3040.1994.tb00278.x
- Casasoli, M., Spadoni, S., Lilley, K. S., Cervone, F., De Lorenzo, G., and Mattei, B. (2008). Identification by 2-D DIGE of apoplastic proteins regulated by oligogalacturonides in *Arabidopsis thaliana*. *Proteomics* 8, 1042–1054. doi: 10.1002/pmic.200700523
- Covarrubias, A. A., Ayala, J. W., Reyes, J. L., Hernández, M., and Garciarrubio, A. (1995). Cell-wall proteins induced by water deficit in bean (*Phaseolus vulgaris* L.) Seedlings. *Plant Physiol.* 107, 1119–1128.
- Curie, C., and Briat, J. F. (2003). Iron transport and signaling in plants. *Annu. Rev. Plant Biol.* 54, 183–206. doi: 10.1146/annurev.arplant.54.031902.135018
- Dani, V., Simon, W. J., Duranti, M., and Croy, R. R. D. (2005). Changes in the tobacco leaf apoplast proteome in response to salt stress. *Proteomics* 5, 737–745. doi: 10.1002/pmic.200401119
- Dannel, F., Pfeffer, H., and Marschner, H. (1995). Isolation of apoplastic fluid from sunflower leaves and its use for studies on influence of Nitrogen supply on apoplastic pH. *J. Plant Physiol.* 146, 273–278. doi: 10.1016/S0176-1617(11)82053-5
- Delanois, B., Colby, T., Belloy, N., Conreux, A., Harzen, A., Baillieul, F., et al. (2013). Large-scale proteomic analysis of the grapevine leaf apoplastic fluid reveals mainly stress-related proteins and cell wall modifying enzymes. *BMC Plant Biol.* 13:24. doi: 10.1186/1471-2229-13-24
- Dietz, K. J. (1997). Functions and responses of the leaf apoplast under stress. *Prog. Bot.* 58, 221–254. doi: 10.1007/978-3-642-60458-4_9
- Donnini, S., Castagna, A., Ranieri, A., and Zocchi, G. (2009). Differential responses in pear and quince genotypes induced by Fe deficiency and bicarbonate. *J. Plant Physiol.* 166, 1181–1193. doi: 10.1016/j.jplph.2009.01.007
- Eichert, T., Peguero-Pina, J. J., Gil-Pelegrín, E., Heredia, A., and Fernández, V. (2010). Effects of iron chlorosis and iron resupply on leaf xylem architecture, water relations, gas exchange and stomatal performance of field-grown peach (*Prunus persica*). *Physiol. Plant.* 138, 48–59. doi: 10.1111/j.1399-3054.2009.01295.x
- Eide, D., Broderius, M., Fett, J., and Guerinot, M. L. (1996). A novel iron-regulated metal transporter from plants identified by functional expression in yeast. *Proc. Natl. Acad. Sci. U.S.A.* 93, 5624–5628. doi: 10.1073/pnas.93.11.5624
- Emanuelsson, O., Brunak, S., Von Heijne, G., and Nielsen, H. (2007). Locating proteins in the cell using TargetP, SignalP and related tools. *Nat. Protoc.* 2, 953–971. doi: 10.1038/nprot.2007.131
- Fecht-Christoffers, M. M., Braun, H.-P., Lemaitre-Guillier, C., Vandorselaer, A., and Horst, W. J. (2003). Effect of Manganese toxicity on the proteome of the leaf apoplast in cowpea. *Plant Physiol.* 133, 1935–1946. doi: 10.1104/pp.103.029215
- Fernández, V., Eichert, T., Del Río, V., López-Casado, G., Heredia-Guerrero, J. A., Abadía, A., et al. (2008). Leaf structural changes associated with iron deficiency chlorosis in field-grown pear and peach: physiological implications. *Plant Soil* 311, 161–172. doi: 10.1007/s11104-008-9667-4
- Floerl, S., Druebert, C., Majcherczyk, A., Karlovsky, P., Kues, U., and Polle, A. (2008). Defence reactions in the apoplastic proteome of oilseed rape (*Brassica napus* var. *napus*) attenuate *Verticillium longisporum* growth but not disease symptoms. *BMC Plant Biol.* 8:129. doi: 10.1186/1471-2229-8-129
- Floerl, S., Majcherczyk, A., Possienke, M., Feussner, K., Tappe, H., Gatz, C., et al. (2012). *Verticillium longisporum* infection affects the leaf apoplastic proteome, metabolome, and cell wall properties in *Arabidopsis thaliana*. *PLoS ONE* 7:e31435. doi: 10.1371/journal.pone.0031435
- Fox, T. C., and Guerinot, M. L. (1998). Molecular biology of cation transport in plants. *Ann. Rev. Plant Physiol. Plant Mol. Biol.* 49, 669–696. doi: 10.1146/annurev.arplant.49.1.669
- González-Vallejo, E. B., Morales, F., Cistué, L., Abadía, A., and Abadía, J. (2000). Iron deficiency decreases the Fe(III)-chelate reducing activity of leaf protoplasts. *Plant Physiol.* 122, 337–344. doi: 10.1104/pp.122.2.337
- Goulet, C., Goulet, C., Goulet, M.-C., and Michaud, D. (2010). 2-DE proteome maps for the leaf apoplast of *Nicotiana benthamiana*. *Proteomics* 10, 2536–2544. doi: 10.1002/pmic.200900382
- Griffith, M., Ala, P., Yang, D. S. C., Hon, W.-C., and Moffatt, B. A. (1992). Antifreeze protein produced endogenously in winter rye leaves. *Plant Physiol.* 100, 593–596. doi: 10.1104/pp.100.2.593
- Hartung, W., Weiler, W. E., and Radin, J. W. (1992). Auxin and cytokinins in the apoplastic solution of dehydrated cotton leaves. *J. Plant Physiol.* 140, 324–327. doi: 10.1016/S0176-1617(11)81086-2
- Jeong, J., Cohu, C., Kerkeb, L., Pilon, M., Connolly, E. L., and Guerinot, M. L. (2008). Chloroplast Fe(III) chelate reductase activity is essential for seedling viability under iron limiting conditions. *Proc. Natl. Acad. Sci. U.S.A.* 105, 10619–10624. doi: 10.1073/pnas.0708367105
- Jeong, J., and Connolly, E. L. (2009). Iron uptake mechanisms in plants: functions of the FRO family of ferric reductases. *Plant Sci.* 176, 709–714. doi: 10.1016/j.plantsci.2009.02.011
- Jorrín-Novo, J. V., Maldonado, A. M., Echevarría-Zomeño, S., Valledor, L., Castillejo, M. A., Curto, M., et al. (2009). Plant proteomics update (2007–2008): second-generation proteomic techniques, an appropriate experimental design, and data analysis to fulfill MIAPE standards, increase plant proteome coverage and expand biological knowledge. *J. Proteomics* 72, 285–314. doi: 10.1016/j.jpro.2009.01.026
- Karhuma, P., Leinonen, J., Parkkila, S., Kaunisto, K., Tapanainen, J., and Rajaniemi, H. (2001). The identification of secreted carbonic anhydrase VI as a constitutive glycoprotein of human and rat milk. *Proc. Natl. Acad. Sci. U.S.A.* 98, 11604–11608. doi: 10.1073/pnas.121172598
- Kim, J. Y., Wu, J., Kwon, S. J., Oh, H., Lee, S. E., Kim, S. G., et al. (2014). Proteomics of rice and *Cochliobolus miyabeanus* fungal interaction: insight into proteins at intracellular and extracellular spaces. *Proteomics* 14, 2307–2318. doi: 10.1002/pmic.201400066
- Kim, S. G., Wang, Y., Lee, K. H., Park, Z.-Y., Park, J., Wu, J., et al. (2013). In-depth insight into *in vivo* apoplastic secretome of rice-*Magnaporthe oryzae* interaction. *J. Proteomics* 78, 58–71. doi: 10.1016/j.jpro.2012.10.029
- Kurepa, J., and Smalle, J. A. (2008). Structure, function and regulation of plant proteasomes. *Biochimie* 90, 324–335. doi: 10.1016/j.biochi.2007.07.019
- Larbi, A., Abadía, A., Morales, F., and Abadía, J. (2004). Fe resupply to Fe-deficient sugar beet plants leads to rapid changes in the violaxanthin cycle and other photosynthetic characteristics without significant *de novo* chlorophyll synthesis. *Photosynth. Res.* 79, 59–69. doi: 10.1023/B:PRES.0000011919.35309.5e
- Lattanzio, G., Andaluz, S., Matros, A., Calvete, J. J., Kehr, J., Abadía, A., et al. (2013). Protein profile of *Lupinus texensis* phloem sap exudates: searching for Fe- and Zn-containing proteins. *Proteomics* 13, 2283–2296. doi: 10.1002/pmic.201200515
- Leinonen, J., Parkkila, S., Kaunisto, K., Koivunen, P., and Rajaniemi, H. (2001). Secretion of carbonic anhydrase isoenzyme VI (CA VI) from human and rat lingual serous von Ebner's glands. *J. Hist. Cyto.* 49, 657–662. doi: 10.1177/002215540104900513
- Lohaus, G., Pennewiss, K., Sattelmacher, B., Hussmann, M., and Hermann Muehling, K. (2001). Is the infiltration-centrifugation technique appropriate for the isolation of apoplastic fluid? A critical evaluation with different plant species. *Physiol. Plant.* 111, 457–465. doi: 10.1034/j.1399-3054.2001.1110405.x
- López-Millán, A.-F., Grusak, M. A., Abadía, A., and Abadía, J. (2013). Iron deficiency in plants: an insight from proteomic approaches. *Front. Plant Sci.* 4:254. doi: 10.3389/fpls.2013.00254
- López-Millán, A. F., Morales, F., Abadía, A., and Abadía, J. (2000a). Effects of iron deficiency on the composition of the leaf apoplastic fluid and xylem sap in sugar beet. Implications for Iron and Carbon transport. *Plant Physiol.* 124, 873–884. doi: 10.1104/pp.124.2.873
- López-Millán, A. F., Morales, F., Andaluz, S., Gogorcena, Y., Abadía, A., Rivas, J. D. L., et al. (2000b). Responses of sugar beet roots to Iron deficiency. Changes in Carbon assimilation and Oxygen use. *Plant Physiol.* 124, 885–898. doi: 10.1104/pp.124.2.885
- Lucas, W. J., Groover, A., Lichtenberger, R., Furuta, K., Yadav, S.-R., Helariutta, Y., et al. (2013). The plant vascular system: evolution, development and functions. *J. Integr. Plant Biol.* 55, 294–388. doi: 10.1111/jipb.12041
- Minic, Z. (2008). Physiological roles of plant glycoside hydrolases. *Planta* 227, 723–740. doi: 10.1007/s00425-007-0668-y

- Mukherjee, I., Campbell, N., Ash, J., and Connolly, E. (2006). Expression profiling of the Arabidopsis ferric chelate reductase (FRO) gene family reveals differential regulation by iron and copper. *Planta* 223, 1178–1190. doi: 10.1007/s00425-005-0165-0
- Nikolic, M., and Römheld, V. (1999). Mechanism of Fe uptake by the leaf symplast: is Fe inactivation in leaf a cause of Fe deficiency chlorosis? *Plant Soil* 215, 229–237. doi: 10.1023/A:1004786211779
- Nikolic, M., and Römheld, V. (2007). “The dynamics of iron in the leaf apoplast,” in *The Apoplast of Higher Plants: Compartment of Storage, Transport and Reactions*, eds B. Sattelmacher and W. J. Horst (Heidelberg: Springer), 353–371.
- Numan, M., and Bhosle, N. (2006). α -L-Arabinofuranosidases: the potential applications in biotechnology. *J. Ind. Microbiol. Biotechnol.* 33, 247–260. doi: 10.1007/s10295-005-0072-1
- Parkhurst, D. (1982). Stereological methods for measuring internal leaf structural variables. *Am. J. Bot.* 69 31–39. doi: 10.2307/2442829
- Pearce, G., Yamaguchi, Y., Barona, G., and Ryan, C. A. (2010). A subtilisin-like protein from soybean contains an embedded, cryptic signal that activates defense-related genes. *Proc. Natl. Acad. Sci. U.S.A.* 107, 14921–14925. doi: 10.1073/pnas.1007568107
- Pechanova, O., Hsu, C.-Y., Adams, J., Pechan, T., Vandervelde, L., Drnevich, J., et al. (2010). Apoplast proteome reveals that extracellular matrix contributes to multistress response in poplar. *BMC Genomics* 11:674. doi: 10.1186/1471-2164-11-674
- Petriccione, M., Salzano, A. M., Di Cecco, I., Scaloni, A., and Scortichini, M. (2014). Proteomic analysis of the *Actinidia deliciosa* leaf apoplast during biotrophic colonization by *Pseudomonas syringae* pv. actinidiae. *J. Proteomics* 101, 43–62. doi: 10.1016/j.jprot.2014.01.030
- Rellán-Álvarez, R., Andaluz, S., Rodríguez-Celma, J., Wohlgemuth, G., Zocchi, G., Álvarez-Fernández, A., et al. (2010). Changes in the proteomic and metabolic profiles of *Beta vulgaris* root tips in response to iron deficiency and resupply. *BMC Plant Biol.* 10:120. doi: 10.1186/1471-2229-10-120
- Robinson, N. J., Procter, C. M., Connolly, E. L., and Guerinot, M. L. (1999). A ferric-chelate reductase for iron uptake from soils. *Nature* 397, 694–697. doi: 10.1038/17800
- Rodríguez-Celma, J., Lattanzio, G., Grusak, M. A., Abadía, A., Abadía, J., and López-Millán, A.-F. (2011). Root responses of *Medicago truncatula* plants grown in two different Iron deficiency conditions: changes in root protein profile and riboflavin biosynthesis. *J. Proteome Res.* 10, 2590–2601. doi: 10.1021/pr2000623
- Rombolà, A. D., and Tagliavini, M. (2006). “Iron nutrition in plants and rhizospheric microorganisms,” in *Iron Nutrition of Fruit Tree Crops*, eds L. L. Barton and J. Abadía (Dordrecht: Springer), 61–83.
- Römheld, V., and Marschner, H. (1986). Evidence for a specific uptake system for Iron phytosiderophores in roots of grasses. *Plant Physiol.* 80, 175–180. doi: 10.1104/pp.80.1.175
- Sampedro, J., Sieiro, C., Revilla, G., González-Villa, T., and Zarra, I. (2001). Cloning and expression pattern of a gene encoding an α -xylosidase active against xyloglucan oligosaccharides from Arabidopsis. *Plant Physiol.* 126, 910–920. doi: 10.1104/pp.126.2.910
- Santi, S., Cesco, S., Varanini, Z., and Pinton, R. (2005). Two plasma membrane H⁺-ATPase genes are differentially expressed in iron-deficient cucumber plants. *Plant Physiol. Biochem.* 43, 287–292. doi: 10.1016/j.plaphy.2005.02.007
- Santi, S., and Schmidt, W. (2008). Laser microdissection-assisted analysis of the functional fate of iron deficiency-induced root hairs in cucumber. *J. Exp. Bot.* 59, 697–704. doi: 10.1093/jxb/erm351
- Santi, S., and Schmidt, W. (2009). Dissecting iron deficiency-induced proton extrusion in Arabidopsis roots. *New Phytol.* 183, 1072–1084. doi: 10.1111/j.1469-8137.2009.02908.x
- Schmidt, W. (1999). Mechanisms and regulation of reduction-based iron uptake in plants. *New Phytol.* 141, 1–26. doi: 10.1046/j.1469-8137.1999.00331.x
- Shenton, M., Berberich, T., Kamo, M., Yamashita, T., Taira, H., and Terauchi, R. (2012). Use of intercellular washing fluid to investigate the secreted proteome of the rice-*Magnaporthe* interaction. *J. Plant Res.* 125, 311–316. doi: 10.1007/s10265-012-0473-y
- Soares, N. C., Francisco, R., Ricardo, C. P., and Jackson, P. A. (2007). Proteomics of ionically bound and soluble extracellular proteins in *Medicago truncatula* leaves. *Proteomics* 7, 2070–2082. doi: 10.1002/pmic.200600953
- Soares, N. C., Francisco, R., Vielba, J. M., Ricardo, C. N. P., and Jackson, P. A. (2009). Associating wound-related changes in the apoplast proteome of *Medicago* with early steps in the ROS signal-transduction pathway. *J. Proteome Res.* 8, 2298–2309. doi: 10.1021/pr8009353
- Starrach, N., and Mayer, W. (1989). Changes of the apoplasmic pH and K⁺ concentration in the *Phaseolus pulvinus* *in situ* in relation to rhythmic leaf movements. *J. Exp. Bot.* 40, 865–873. doi: 10.1093/jxb/40.8.865
- Steudle, E., Smith, J. A. C., and Lüttge, U. (1980). Water-relation parameters of individual mesophyll cells of *Kalanchoë daigremontiana*. *Plant Physiol.* 66, 1155–1163. doi: 10.1104/pp.66.6.1155
- Tachi, H., Fukuda-Yamada, K., Kojima, T., Shiraiwa, M., and Takahara, H. (2009). Molecular characterization of a novel soybean gene encoding a neutral PR-5 protein induced by high-salt stress. *Plant Physiol. Biochem.* 47, 73–79. doi: 10.1016/j.plaphy.2008.09.012
- Vakhmistrov, D. B. (1967). Localization of the free space in the barley roots. *Fiziologiya Rastenii* 14, 397–404.
- Van Der Hoorn, R. A., and Jones, J. D. (2004). The plant proteolytic machinery and its role in defence. *Curr. Opin. Plant Biol.* 7, 400–407. doi: 10.1016/j.pbi.2004.04.003
- Vigani, G. (2012). Discovering the role of mitochondria in the iron deficiency-induced metabolic responses of plants. *J. Plant Physiol.* 169, 1–11. doi: 10.1016/j.jplph.2011.09.008
- Witzel, K., Shahzad, M., Matros, A., Mock, H.-P., and Muhling, K. (2011). Comparative evaluation of extraction methods for apoplastic proteins from maize leaves. *Plant Methods* 7:48. doi: 10.1186/1746-4811-7-48
- Wolf, O., Munns, R., Tonnet, M. L., and Jeschke, W. D. (1990). Concentrations and transport of solutes in xylem and phloem along the leaf axis of NaCl-treated *Hordeum vulgare*. *J. Exp. Bot.* 41, 1133–1141. doi: 10.1093/jxb/41.9.1133
- Xia, Y., Suzuki, H., Borevitz, J., Blount, J., Guo, Z., Patel, K., et al. (2004). An extracellular aspartic protease functions in Arabidopsis disease resistance signaling. *EMBO J.* 23, 980–988. doi: 10.1038/sj.emboj.7600086
- Zhang, F.-S., Römheld, V., and Marschner, H. (1991). Role of the root apoplast for Iron acquisition by wheat plants. *Plant Physiol.* 97, 1302–1305. doi: 10.1104/pp.97.4.1302
- Zocchi, G. (2006). “Metabolic changes in iron-stressed dicotyledonous plants,” in *Iron Nutrition in Plants and Rhizospheric Microorganisms*, eds L. L. Barton and J. Abadía (Dordrecht: Springer), 359–370.

Conflict of Interest Statement: The authors declare that the research was conducted in the absence of any commercial or financial relationships that could be construed as a potential conflict of interest.

Copyright © 2015 Ceballos-Laita, Gutierrez-Carbonell, Lattanzio, Vázquez, Contreras-Moreira, Abadía, Abadía and López-Millán. This is an open-access article distributed under the terms of the Creative Commons Attribution License (CC BY). The use, distribution or reproduction in other forums is permitted, provided the original author(s) or licensor are credited and that the original publication in this journal is cited, in accordance with accepted academic practice. No use, distribution or reproduction is permitted which does not comply with these terms.